Dopazo C, Cifuentes L, Chakraborty N.

Vorticity budgets in premixed combusting turbulent flows at different Lewis numbers.

***Physics of Fluids* 2017, 29, 045106.**

Vorticity budgets in premixed combusting turbulent flows at different Lewis numbers

Cesar Dopazo,[1] Luis Cifuentes,[1,2,*] and Nilanjan Chakraborty[3]

[1]*School of Engineering and Architecture - Fluid Mechanics Area, University of Zaragoza, C/ Maria de Luna 3, Zaragoza 50018, Spain*

[2]*Institute for Combustion and Gasdynamics (IVG), Chair for Fluid Dynamics, University of Duisburg-Essen, Duisburg 47048, Germany*

[3]*School of Mechanical and Systems Engineering, Newcastle University, Claremont Road Newcastle-Upon-Tyne NE1 7RU, UK*

(Dated: February 19, 2017)

Abstract

A Direct Numerical Simulations (DNS) database of statistically planar turbulent premixed flames using a simple Arrhenius type irreversible chemistry for different values of global Lewis numbers, Le, (0.34, 0.60, 0.80, 1.00, 1.20) has been examined to analyze the effects of Le on vorticity transport within the flame. To meet this objective a general enstrophy conservation equation has been considered, which distinctly describes contributions from vortex-stretching, destruction by volumetric dilatation rates, baroclinic and viscous force torques, viscous transport and dissipation. The average statistical behavior of the various contributions conditioned upon the value of the reaction progress variable, c, has been analyzed in the preheat and reacting regions of the flame. The mean values of enstrophy monotonically decays with c from fresh reactants toward hot products for Le equal to 0.8, 1.0 and 1.2; vortex-stretching and viscous dissipation are the leading contributors, while the remaining contributions are slightly smaller although non negligible. By contrast, the mean value of enstrophy decreases from the leading edge before increasing up to the trailing edge of the flame; in these cases, the mean value of baroclinic torque is significantly greater than the other contributions in most of the preheat and reacting regions; vortex-stretching, destruction by volumetric dilatation rates and viscous transport and dissipation remain comparable over most of the flame. An explanation for the significant qualitative and quantitative differences in the enstrophy transport, taking place for Le between 0.6 and 0.8 for the given turbulence intensity, is sought in terms of the alignments of vorticity and the gradients of density, pressure, temperature and reaction progress variable.The transport statistics of the enstrophies of the vorticity vector components tangential and normal to iso-scalar surfaces, $c(\mathbf{x}, t) =$ constant, provide further insight into the mechanisms of the differences in the enstrophy transport in response to the changes in global Lewis number.

Keywords: Vorticity; enstrophy; turbulent premixed flame; direct numerical simulations; Lewis number; combustion

*Electronic address: luis.cifuentes@uni-due.de

I. INTRODUCTION

Vorticity and enstrophy are fundamental attributes of turbulent flows [1] and the investigation of its dynamics is of a paramount interest [2]. Therefore, vorticity and enstrophy budgets must be unmistakably related to those of kinetic energy and its dissipation rate within the flame. The long-standing issue of flame-generated turbulence in combusting flows, which has been experimentally and numerically investigated [3–14], might find sound answers by examining the vorticity dynamics. A definition of flame-generated turbulence has been proposed, determining experimentally that "in some cases the flame damps the turbulence whereas in most other instances it generates additional turbulence", estimating that the "total magnitude of the relative flame-generated turbulence intensity does not exceed about 12%" [6]. The turbulent kinetic energy budget for a premixed methane-air flame has been investigated through the measurement of the various terms, finding that flame-generated turbulence increases with heat release [7]. On the other hand, Favre averaged turbulent kinetic energy in premixed turbulent flames have been computed, showing that for large ratios of unburned reactants and burned products densities the axial turbulent kinetic energy "increases by a factor of 17 through the flame, while the variances of the other two components increase by just 50%" [8]. A DNS database of a turbulent premixed flame has been used to understand the mechanisms of flame-generated turbulence and assess the performance of zone-conditional two-fluid equations [14].

Several features of vorticity and its alignment with the eigenvectors of the strain rate tensor for turbulent non-premixed [15–18] and premixed [19–28] flames have been scrutinized. The important effects of the Lewis number, Le, on the geometry and statistical features of turbulent premixed flames has been unveiled using DNS [29, 30]; Chakraborty [31] has shown that the vorticity statistics and its alignment with the principal directions of strain is significantly affected by the values of Le, with profound differences for the "thin reaction zone" and the "corrugated flamelet" regimes. Chakraborty et al. [32] have examined DNS data sets for a statistically planar turbulent premixed flames to investigate the anisotropic behavior within the flame brush due to the baroclinic torque of the average vorticity components, and to reveal that the correlation between the fluctuations of enstrophy and dilatation rate play an important role in determining the material derivative of enstrophy based on the mean flow in the case of a low Le.

Gorski and Bernard [33] proposed an enstrophy transport equation in the context of RANS modeling. Bobbitt et al. [34] examined DNS data sets to investigate changes in turbulence (linearly forced) characteristics across high Karlovitz (Ka) number n-heptane/air premixed flames, modeled with a 35-species finite-rate chemical mechanism; they found vorticity to scale with the Kolmogorov time micro-scale and vortex-stretching and viscous dissipation to be the leading terms in the enstrophy transport equation. Bobbitt and Blanquart [35] used the same DNS database to investigate the isotropy of the smallest turbulent scales through the analysis of the vorticity vector; vortex-stretching is responsible for anisotropy, which reduces as Ka and the integral-scale/flame thickness ratio increases. For high Ka the local dynamics of vorticity and stretching resembles that of homogeneous isotropic turbulence, whereas the flame modifies vortex-stretching and vorticity alignments with the strain-rate tensor eigenvectors at low Ka. Ranjan et al. [36] used three DNS data sets for freely propagating CH4-air statistically planar premixed flames interacting with a field of decaying homogeneous turbulence to test several LES modelling strategies with finite-rate chemistry; three different combinations of low, intermediate and high Ka, Re and turbulence r.m.s/laminar flame-thickness, and comparable integral-scale/flame thickness ratios were explored; they obtained that the characteristic length of vorticity structures increases across the flames and that vortex-stretching and "viscous dissipation" are leading terms for intermediate and high Ka, while the baroclinic torque plays a minor role and the dilatation term can be negative for high Ka.

The aim of the present analysis is to investigate the influence Lewis number on the instantaneous vorticity and enstrophy fields of a turbulent premixed statistically planar flame. An existing DNS database [37–39] for statistically planar turbulent premixed flames with a simple one-step Arrhenius-type chemical conversion has been examined, and the various terms in the enstrophy transport equation have been computed across the flame. There have been several previous analyses [29, 30, 40–42] where single-step chemistry is used to analyse the effects of global Lewis number in isolation, and the same approach has been adopted here. The statistical behaviours of vorticity and enstrophy transport in premixed turbulent flames are principally driven by fluid-dynamics, and the pressure and density gradients induced by the thermal field. These aspects are influenced by global dependences of the chemical reaction rate on reaction progress variable and temperature fields, which are satisfactorily captured by simple one-step chemistry; this is confirmed by comparing

the reaction progress variable dependence of chemical reaction rate in Chakraborty and Cant [43] and Chakraborty et al. [44]. Similarly, the statistics of scalar-gradients obtained from simple chemistry DNS [45–47] are found to be qualitatively similar to the corresponding results from detailed chemistry DNS data [44, 48, 49].

This work presents a detailed parametric DNS data analysis to scrutinize the effects of global Lewis number on the statistical behaviour of enstrophy transport across statistically planar turbulent premixed flames. Some objectives of this research are:

- to present simple vorticity and enstrophy transport equations with every term having a clear physical meaning, and also to decompose the total enstrophy into the additive contributions of the vorticity vector components normal and tangential to iso-scalar surfaces obtaining their evolution equations,
- to examine the relative importance of the various terms contributing to the total, normal and tangential enstrophies for different Lewis numbers,
- to explain the increasing importance of the baroclinic torque as the Lewis number decreases and the influences of diffusive-thermal instability aftereffects manifest; alignments among the various vector fields contributing to the baroclinic torque in the enstrophy transport equation are scrutinized, and its relative contributions to normal and tangential enstrophies are obtained.

This work explores the influence of the global Lewis number on the flow vorticity dynamics across statistically planar turbulent premixed flames. Causes for the large values of the mean baroclinic torque conditional upon the reaction progress variable for small values of global Lewis number are investigated; alignments among the various vector fields contributing to the baroclinic torque in the enstrophy transport equation are scrutinized. Contributions to the transport equations of enstrophies ascribed to the vorticity components normal and tangential to iso-scalar surfaces are also examined and yield further insight into the vorticity evolution within turbulent flames.

Section II concentrates on the derivation of the total enstrophy transport equation and of that of its additive constituents due to the vorticity components tangential and normal to iso-scalar surfaces. Some brief information on the numerics of the DNS code used to

generate the analyzed dataset is provided in Section III. Main results are presented and discussed in Section IV. Conclusions are summarized in Section V.

II. MATHEMATICAL DESCRIPTION

A vorticity transport equation can be derived, starting from the flow momentum equation,

$$\frac{\partial u_i}{\partial t} + u_j \frac{\partial u_i}{\partial x_j} = -\frac{1}{\rho}\frac{\partial p}{\partial x_i} + \frac{1}{\rho}\frac{\partial \tau_{ij}}{\partial x_j} \,, \tag{1}$$

where p is the pressure and the viscous stress tensor, τ_{ij}, obeys the Navier-Poisson constitutive relation

$$\tau_{ij} = 2\mu S_{ij} - \frac{2}{3}\mu S_{kk}\delta_{ij} \,, \tag{2}$$

where μ is the dynamic viscosity coefficient, taken as a constant. Here, S_{ij} is the rate of strain tensor defined by

$$S_{ij} = \frac{1}{2}\left(\frac{\partial u_i}{\partial x_j} + \frac{\partial u_j}{\partial x_i}\right) \,. \tag{3}$$

Applying the curl operator, $\varepsilon_{ijk}\partial(\ )/\partial x_j$, to equation (1), it is possible to obtain the vorticity transport equation

$$\begin{aligned}\frac{\partial \omega_i}{\partial t} + u_j \frac{\partial \omega_i}{\partial x_j} =& S_{ij}\omega_j - S_{jj}\omega_i + \varepsilon_{ijk}\frac{1}{\rho^2}\frac{\partial \rho}{\partial x_j}\frac{\partial p}{\partial x_k} \\ &- \varepsilon_{ijk}\frac{1}{\rho^2}\frac{\partial \rho}{\partial x_j}\frac{\partial \tau_{kl}}{\partial x_l} + \nu\nabla^2\omega_i \,.\end{aligned} \tag{4}$$

The vorticity vector is defined by $\omega_i = \varepsilon_{ijk}\partial u_k/\partial x_j$ and ε_{ijk} is the Levi-Civitta alternating tensor. The first term on the right side of equation (4) represents the vortex-stretching, while the second one stands for the vorticity annihilation/generation by positive/negative volumetric dilatation rates. The third and fourth terms embody the torques by pressure and viscous forces, respectively. The fifth term denotes the viscous diffusion of vorticity.

Multiplying equation (4) by ω_i, one can readily obtain a transport equation for the enstrophy, $E = \omega_i\omega_i/2$,

$$\frac{\partial E}{\partial t} + u_j \frac{\partial E}{\partial x_j} = \underbrace{\omega_i S_{ij} \omega_j}_{T_1} - \underbrace{2E S_{jj}}_{T_2} + \underbrace{\varepsilon_{ijk} \frac{\omega_i}{\rho^2} \frac{\partial \rho}{\partial x_j} \frac{\partial p}{\partial x_k}}_{T_3}$$
$$\underbrace{- \varepsilon_{ijk} \frac{\omega_i}{\rho^2} \frac{\partial \rho}{\partial x_j} \frac{\partial \tau_{kl}}{\partial x_l}}_{T_4} + \underbrace{\frac{\mu}{\rho} (\nabla^2 E)}_{T_5} - \underbrace{\frac{\mu}{\rho} \left(\frac{\partial \omega_i}{\partial x_j} \frac{\partial \omega_i}{\partial x_j} \right)}_{T_6} . \tag{5}$$

In equation (5), T_1 is the enstrophy generation by vortex-stretching, T_2 is the enstrophy annihilation/production by the volumetric dilatation rate, T_3 and T_4 are the contributions to E of pressure (baroclinic) and viscous torques, respectively, T_5 is the viscous transport of enstrophy and T_6 its viscous dissipation rate. The various terms $T_1 - T_6$ quantify not only the magnitude of the different vectors and tensors contributing to them, but also of the alignment of the vectorial terms on the right side of Eq. (4) with the vorticity vector; for example, $\boldsymbol{\omega} \cdot (\mathbf{S} \cdot \boldsymbol{\omega}) = |\boldsymbol{\omega}||\mathbf{S} \cdot \boldsymbol{\omega}| \cos(\boldsymbol{\omega}, (\mathbf{S} \cdot \boldsymbol{\omega}))$ depends on the magnitudes of the vorticity and vortex-stretching vectors and on their alignment, given by the cosine of the angle between them.

The local vorticity vector can be decomposed into its components normal and tangential to an iso-scalar surface $c(\mathbf{x}, t) =$ constant [32],

$$\omega_i = (\omega_j n_j)\, n_i + (\delta_{ij} - n_i n_j)\, \omega_j \, , \tag{6}$$

c is the reaction progress variable with local unit normal vector, $\mathbf{n}$, defined by $\mathbf{n} = -\nabla c / |\nabla c|$.

The enstrophy associated to the normal component of the vorticity is

$$E_N = \frac{1}{2} (\omega_j n_j) (\omega_k n_k) \, , \tag{7}$$

whereas that due to the tangential component is

$$E_T = \frac{1}{2} [(\delta_{ij} - n_i n_j)\omega_j] [(\delta_{ik} - n_i n_k)\omega_k] \, . \tag{8}$$

Therefore, one can write the following: $E = \omega_i \omega_i / 2 = E_N + E_T$.

A transport equation for the enstrophy associated to the normal component of the vorticity can be readily derived

$$\frac{DE_N}{Dt} = \underbrace{2\left(n_i S_{ij}\omega_j + V\omega_i\frac{\partial n_i}{\partial x_N}\right)\omega_N}_{T_{N1}} - \underbrace{\left(S_{jj}+a_N\right)\left(\omega_N\right)^2}_{T_{N2}}$$
$$+ \underbrace{n_i\varepsilon_{ijk}\frac{1}{\rho^2}\frac{\partial\rho}{\partial x_j}\frac{\partial p}{\partial x_k}\omega_N}_{T_{N3}} - \underbrace{n_i\varepsilon_{ijk}\frac{1}{\rho^2}\frac{\partial\rho}{\partial x_j}\frac{\partial\tau_{kl}}{\partial x_l}\omega_N}_{T_{N4}} + \underbrace{\left(n_i\nu\nabla^2\omega_i\right)\omega_N}_{T_{N5}} . \quad (9)$$

The first term on the right side represent the vortex-stretching contribution to E_N and the second its annihilation by volumetric dilatation. The third and fourth terms are the generation of E_N by the baroclinic and the viscous-force torques. The last term contains both viscous transport and dissipation of E_N.

Similarly, a transport equation for E_T can be obtained from its definition. However, subtracting Eq. (9) from Eq.(5), an alternative transport equation for E_T is derived.

III. DNS DATASETS EXAMINED

A DNS database of freely propagating statistically planar turbulent premixed flames with Le =0.34, 0.6, 0.8, 1.0 and 1.2 is examined. It was generated using a three-dimensional variable-density code SENGA [37], which solved non-dimensional mass, momentum, energy and reaction progress variable conservation equations. This database has been used in several previous analyses and provided important insights into several aspects of combustion science and modeling [38, 39].

It can be stated that the unity Lewis number flames are analogous to the stoichiometric CH4-air flame, whereas the Lewis number 0.34 case is representative of a lean H2-air mixture. The Lewis number 0.6 and 0.8 flames are representative of H2-blended CH4-air mixtures (e.g., 20% and 10%, by volume H2-blended CH4-air flames with overall equivalence ratio of 0.6) and the Lewis number 1.2 case is representative of a hydrocarbon-air mixture involving a fuel heavier than CH4 (e.g., ethylene-air mixture with equivalence ratio of 0.7) [50–53]. Furthermore, the range of Lewis numbers considered here is comparable to that explored by Trouvé and Poinsot [41].

A. Dimensionless equations

The full set of governing equations is made dimensionless using reference characteristic variables. The non-dimensional mass, momentum, energy and progress variable transport equations are given by [37]:

$$\frac{\partial \rho^+}{\partial t^+} + \frac{\partial (\rho^+ u_i^+)}{\partial x_i^+} = 0 \,, \tag{10}$$

$$\frac{\partial (\rho^+ u_i^+)}{\partial t^+} + \frac{\partial (\rho^+ u_k^+ u_i)}{\partial x_k} = -\frac{\partial P^+}{\partial x_i^+} + \frac{1}{Re}\frac{\partial (\tau_{ki}^+)}{\partial x_k^+} \,, \tag{11}$$

$$\begin{aligned}\frac{(\rho^+ E^+)}{\partial t^+} + \frac{(\rho^+ u_k^+ E^+)}{\partial x_k^+} =& -(\gamma-1)Ma^2\frac{\partial (P^+ u_k)}{\partial x_k^+} + \frac{1}{Re}(\gamma-1)Ma^2\frac{\partial (\tau_{ki}^+ u_i^+)}{\partial x_k^+} \\ &+ \frac{\tau}{RePr}\frac{\partial}{\partial x_k}\left(\lambda\frac{\partial T^+}{\partial x_k^+}\right) - \frac{\tau}{RePr}\frac{\partial}{\partial x_k^+}\left(\rho D\frac{\partial c}{\partial x_k^+}\right) \,,\end{aligned} \tag{12}$$

$$\frac{(\rho^+ c)}{\partial t^+} + \frac{(\rho^+ u_k^+ c)}{\partial x_k^+} = \dot{\omega}^+ + \frac{1}{ReSc}\frac{\partial}{\partial x_k^+}\left(\rho D\frac{\partial c}{\partial x_k^+}\right) \,. \tag{13}$$

All non-dimensional quantities are shown with a + superscript. In eqs. (10)-(13), $Re = \rho_{ref} u_{ref} L_{ref}/\mu_{ref}$ is the nominal Reynolds number, $Ma = u_{ref}/a_{ref}$ is the Mach number, $\gamma = C_p/C_v$ is the ratio of specific heats, Pr is the Prandtl number and $Sc = PrLe$ is the Schmidt number, ρ_{ref}, u_{ref}, L_{ref}, a_{ref} and μ_{ref} are the reference values of density, velocity, length scale, acoustic velocity and viscosity respectively. Here the density, viscosity and acoustic speed of the unburned gas are taken to be ρ_{ref}, μ_{ref} and a_{ref} respectively, and S_L and $10\delta_{th}$ are considered to be u_{ref} and L_{ref}, respectively, where $\delta_{th} = (T_{ad} - T_u)/\max|\nabla T_{ins}|_L$ is the thermal flame thickness, with T_{ins} being the instantaneous dimensional temperature; the subscript "L" refers to unstrained laminar flame quantities. The internal energy $E = C_v T + u_k u_k/2 + H(1-c)$ (where H the heat of reaction per unit mass of reactants consumed) is normalised by $C_p T_0$ in the following manner:

$$E = \frac{1}{\gamma}(1 + \tau T^+) + \frac{1}{2}(\gamma-1)Ma^2 u_k^+ u_k^+ + \tau(1-c) \,. \tag{14}$$

$T^+ = (T - T_u)/(T_{ad} - T_u)$ is the non-dimensional temperature. The gas is assumed to follow

the perfect gas law $P = \rho RT$, which takes the following non-dimensional form:

$$P^+ = \frac{1}{\gamma Ma^2}\rho^+(1+\tau T^+)\,. \tag{15}$$

It can easily be seen from eqs. (10)-(15) that u'/S_L, l/δ_{th}, τ and $Le = Sc/Pr$ are the key non-dimensional parameters which govern the system of equations and explicit values of S_L, T_{ad}, T_u and T_{ac} are not necessary for the purpose of this analysis.

B. Numerical simulation

A planar laminar flame, used as initial condition for the scalar fields, is allowed to interact with the turbulent flow, which is initialized using a precomputed incompressible homogeneous isotropic velocity field [54]. The domain is considered to be periodic in the y and z directions, while partially non-reflecting boundary conditions are imposed in the $x-$direction, using the Navier-Stokes Characteristic Boundary Conditions (NSCBC) approach [54]. In this configuration, no forcing is used to maintain the turbulence level and the flame-turbulence interaction takes place under decaying turbulence, similar to previous analyses [29, 30, 40–42].

Spatial derivatives for the internal grid points are evaluated using a tenth-order central difference scheme, with the order of differentiation dropping gradually to a one-sided second-order scheme at the non-periodic boundaries. A third order explicit Runge-Kutta scheme [55] is used for time advancement.

The chemical mechanism is simplified by using a simple one-step Arrhenius-type chemical conversion for the purpose of computational economy and to explore the effects of the Lewis number, Le, in isolation following several previous analyses [29, 30, 42]. The enstrophy transport is primarily a fluid-dynamic phenomenon, and the combustion process affects the enstrophy transport only through the heat release pattern. In principle, the effects of detailed chemical kinetics are relatively irrelevant because simple chemistry qualitatively captures the heat release pattern within premixed flames.

For the current study, the heat release parameter, $\tau = (T_{ad} - T_u)/T_u$, and the Zel′dovich number, $\beta = T_{ac}(T_{ad} - T_u)/T_{ad}^2$, are set equal to 4.5 and 6.0, respectively; the subscripts "u" and "b" stand for variables in "unburned" and "burnt" gases. T_{ad}, T_u and T_{ac} are the adiabatic flame, the unburned gas and the activation temperatures, respectively. For the

present analysis, the reaction progress variable, c, is defined based on a suitable reactant mass fraction Y_R as:

$$c = \frac{Y_{R_u} - Y_R}{Y_{R_u} - Y_{R_b}} \,. \tag{16}$$

The reaction progress variable vanishes in the fresh reactants and monotonically grows to become unity in the hot products. $c(\mathbf{x}, t)$ obeys the conventional convection-diffusion-reaction equation,

$$\frac{\partial c}{\partial t} + u_j \frac{\partial c}{\partial x_j} = \frac{1}{\rho} \frac{\partial}{\partial x_j} \left(\rho D \frac{\partial c}{\partial x_j} \right) + \dot{\omega}_c \,. \tag{17}$$

The computational domain is taken to be a cube with every side equal to $24.1\delta_{th}$, which is discretised using a uniform grid of $230 \times 230 \times 230$. It is possible to define an alternative flame thickness as $\delta_L = 1/\max|\nabla c|_L$. The thicknesses δ_L and δ_{th} are not equal to each other and $\delta_L > \delta_{th}$ ($\delta_L < \delta_{th}$) for $Le < 1$ ($Le > 1$) flames. For the $Le \approx 1.0$ (e.g., 0.8, 1.0 and 1.2) δ_L and δ_{th} remain comparable (i.e., $\delta_L/\delta_{th} \approx 0.9$, 1.0 and 1.15 for $Le = 1.2$, 1.0 and 0.8), whereas δ_L/δ_{th} is 1.4 and 2.1 for $Le = 0.6$ and 0.34 flames. Thus, in all cases either about 10 or more than 10 grid points within δ_L are taken. For detailed chemistry DNS one has to resolve the reaction layer for intermediate species and thus typically 15 points are kept within the flame thickness, but for simple chemistry DNS 10 grid points often suffices [56]. The flame resolution used in this paper is consistent with existing studies [29, 30, 40–42], which concentrated on the effects of global Lewis number.

The initial r.m.s. velocity to laminar burning velocity and integral length scale to flame thickness ratios of every simulation are taken to be $u'/S_L = 7.5$ and $l/\delta_{th} = 2.45$, respectively, which yield a Damköhler number $Da = (l/\delta_{th})/(u'/S_L) = 0.32$, and a Karlovitz number $Ka = (u'/S_L)^{3/2}(l/\delta_{th})^{-1/2} = 13.12$.

The domain size in the canonical configuration is governed by the necessity of enough number of eddies within the computational domain. For the cases considered here, the initial value of l/δ_{th} is taken to be 2.45 so a domain length of $24.1\delta_{th}$ accommodates 10 integral eddies within every side of the domain. The minimum distance of the $c = 0.99$ iso-surface from the outlet boundary is of the order of $4.0\delta_{th}$ (i.e., greater than or equal to 40 grid points). Reducing the domain size by $1.5\delta_{th}$ on every side had a marginal effect on the statistics (e.g., maximum difference in $|\nabla c|$ values was about 0.5%). The grid spacing

Δx for a $230 \times 230 \times 230$ grid amounts to $\eta = 1.4\Delta x$, and making the grid coarser to $200 \times 200 \times 200$ (which amounts to $\eta = 1.2\Delta x$) did not change the statistical behaviour (e.g., maximum difference in $|\nabla c|$ values was about 0.1%). The domain size remains either comparable or greater than that used in published works [29, 30, 40–42].

In decaying turbulence simulations, the desirable simulation time t_{sim} is given by $t_{sim} \geq \max(t_f, t_c)$ (where $t_f = l/u'$ is the initial eddy turn over time and $t_c = \delta_{th}/S_L$ is the chemical time scale), which guarantees that the statistics can be extracted at a time when the flow field is in principle independent of initial conditions. Here, the simulation time is equal to one chemical time, which corresponds to 3.34 initial integral eddy turnover times. This simulation time is comparable to that in several previous analyses, which contributed to the fundamental understanding of turbulent premixed combustion [29, 30, 42, 57]. The averaging done here is ensemble averaging on a given $c-$isosurface at the time when the statistics were extracted and the same approach was adopted in several previous analyses [45, 57]. All the statistical behaviours shown in the paper remain qualitatively unaltered since halfway through the simulation. The temporal evolution of turbulent flame speed for the cases considered here is provided in Fig. 2(e) of Chakraborty and Cant [39], which is not repeated in this paper for the sake of brevity. The temporal evolution of flame reveals that the turbulent flame speed was not changing rapidly with time for the $Le = 0.8$, 1.0 and 1.2 cases. The effects of the thermo-diffusive instability strengthen with decreasing Lewis number. Thus, a quasi-stationary state is not obtained for the $Le = 0.34$ and 0.6 cases considered here, and perhaps it is not physically sound to expect a quasi-stationary state for all cases. A similar behaviour was reported by Trouvé and Poinsot [41].

The root-mean-square velocity fluctuation in the unburned gas ahead of the flame (evaluated using the samples corresponding to $c < 0.01$.) decayed by about 50%, whereas the integral length scale increased by a factor of 1.7 in comparison to its initial value. The Zel′dovich flame thickness α_{T_0}/S_L (where α_{T_0} is the thermal diffusivity in the unburned gas) scales with δ_{th} (here $\delta_{th} \approx 2\alpha_{T_0}/S_L$), and, thus, the combustion takes place in the 'thickened-wrinkled flame' regime for the values of u'/S_L and l/δ_{th} considered here. The scaling arguments for the regime diagram are strictly valid for unity Lewis number, and, therefore, the non-unity Lewis number flames are nominally within the thin reaction zone regime. It has been demonstrated by Chakraborty and Cant [39] that the magnitude of flame wrinkling in this analysis is at least representative for some laboratory flames [40].

Further information regarding this database can be found elsewhere [9, 31, 38, 57].

IV. RESULTS AND DISCUSSION

The variation of the mean value of $\dot{\omega}_c$ conditional on c for the turbulent flames considered here is shown in Figure 1; illustratively, a preheat region, $0.3 < c < 0.75$, and a burning zone, $0.75 < c < 0.95$, can be delimited, although they are not essential for the results and conclusions of this work. The reactants diffuse faster into the reaction zone than the rate of thermal diffusion for $Le < 1$ flames, which gives rise to higher rate of burning than the corresponding $Le = 1$ flames due to simultaneous presence of high temperature and high reactant concentration in the reaction zone. By contrast, thermal diffusion is faster than the reactant diffusion in the $Le > 1$ flames, which leads to a reduction in the rate of burning due to relatively lower temperature and reactant concentration within the reaction zone in these flames than in the corresponding $Le = 1$ flame. The aforementioned physical mechanisms are responsible for the increasing trend of $\dot{\omega}_c$ with decreasing Le. Table I lists the normalised values of the volume-integrated reaction rate of progress variable R_T/R_L (where $R = \int_V \rho\dot{\omega}_c dV$ and the subscripts T and L are used for turbulent and laminar flame conditions, respectively), which show that R_T/R_L increases significantly with decreasing Le, consistent with the above discussion. Interested readers are referred to Refs. [9, 29–31, 38, 57] and references therein for further discussion on the augmentation of burning rate and flame surface area with decreasing global Lewis number.

Muppala et al. [50] experimentally obtained that $(A_T/A_L - 1)$ scales with $(1/Le)(u'/S_L)^{0.3}Re_t^{0.25}$. For the values of u'/S_L and l/δ_{th} at the time when statistics were extracted (presented in Table 2 in Chakraborty and Cant [58]), the value of $[(A_T/A_L - 1)Le/(u'/S_L)^{0.3}Re_t^{0.25}] \,/\, [(A_T/A_L - 1)Le/(u'/S_L)^{0.3}Re_t^{0.25}]_{(Le=1)}$ remains of order unity (i.e., 1.05, 1.06, 1.02 and 1.03 for the $Le = 0.34$, 0.6, 0.8 and 1.2 flames, respectively) for all the non-unity Lewis number cases, which is in good agreement with the findings of Muppala et al. [50].

Figure 2 presents an instantaneous snapshot of enstrophy $E = \omega_i\omega_i/2$ contours in a plane, midway of the y coordinate of the computational domain, at time $t = \delta_{th}/S_L$ when the statistics were extracted. This instantaneous enstrophy distribution helps to visualize its generation across turbulent premixed flames due to the variation in Le. It is apparent

that a major part of the flame acts as an enstrophy suppressor for the cases with $Le \geq 0.80$. On the contrary, the flame apparently augments the enstrophy of the flow downstream of the flame for the $Le = 0.34$ and 0.6 cases. However, the extent of enstrophy augmentation in the $Le = 0.6$ case is much weaker than in the $Le = 0.34$ flame.

The above observations could be substantiated further from the variations of mean enstrophy, conditioned upon the reaction progress variable, c, as shown in Figure 3. A slight increment of enstrophy for $Le = 0.60$ can be observed within the flame, in the progress variable range $0.3 \leq c \leq 0.95$, but this augmentation of E is particularly pronounced for the $Le = 0.34$ case.

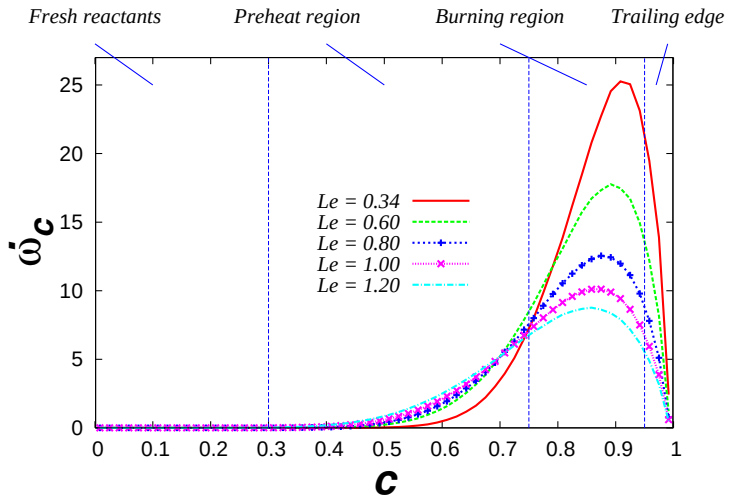

FIG. 1: Variation of mean values of reaction rate, $\dot{\omega}_c = \dot{\omega}/\rho$, conditional upon c, for different Lewis numbers. Dotted lines mark the limits of the four regions of the computational domain.

TABLE I: The effects of Lewis number on normalised volume-integrated reaction rate of progress variable R_T/R_L after 3.34 initial eddy turn over times.

Le	R_T/R_L
0.34	13.70
0.60	4.58
0.80	2.53
1.00	1.83
1.20	1.50

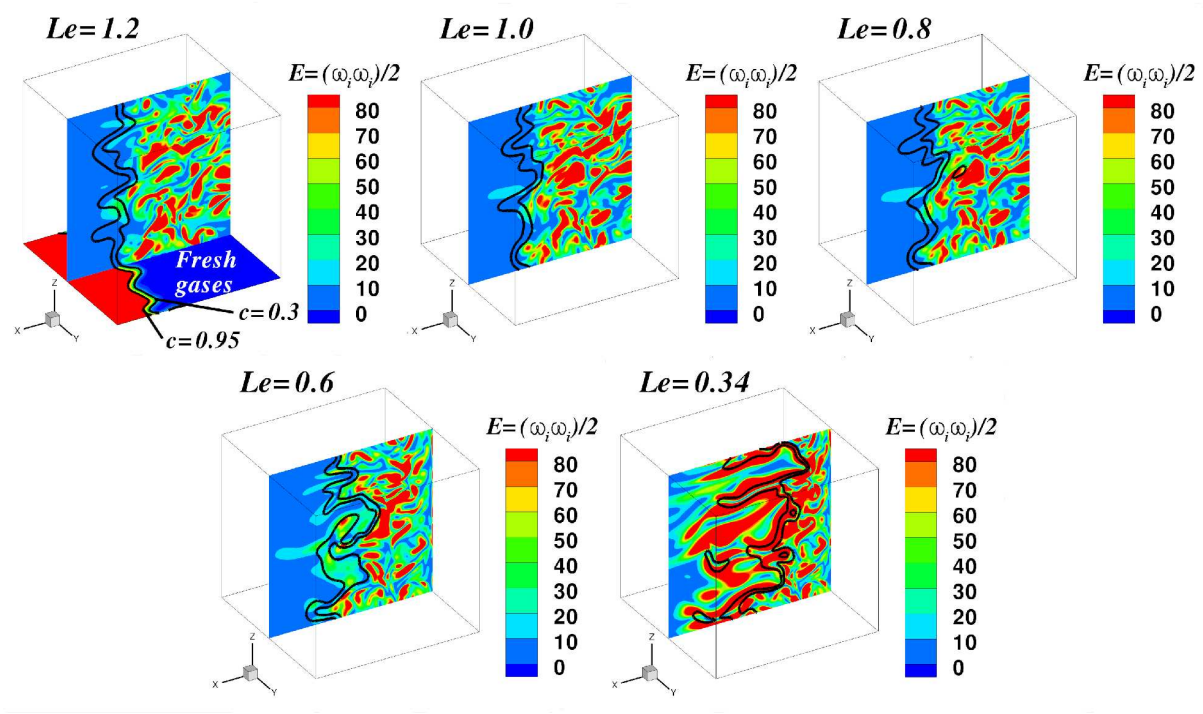

FIG. 2: Instantaneous enstrophy, $E = (\omega_i\omega_i)/2$, at different Lewis numbers. E has been normalized with $(\delta_{th}/S_L)^2$ corresponding to the $Le = 1.0$ flame. Iso-lines of the progress variable c=0.3 and c=0.95 mark the limits for the preheat and burning regions.

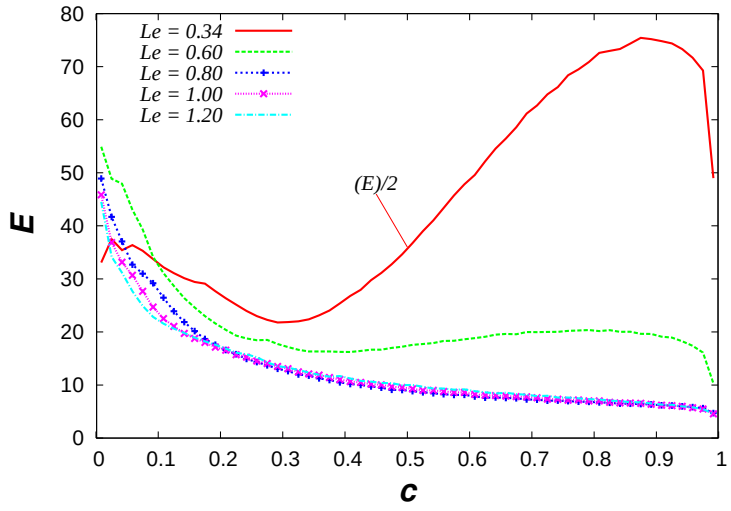

FIG. 3: Mean enstrophy, $E = (\omega_i\omega_i)/2$, conditional upon c, at different Le. The enstrophy E has been normalized with $(\delta_{th}/S_L)^2$ corresponding to the $Le = 1.0$ flame. The mean value of enstrophy for $Le = 0.34$ has been divided by two.

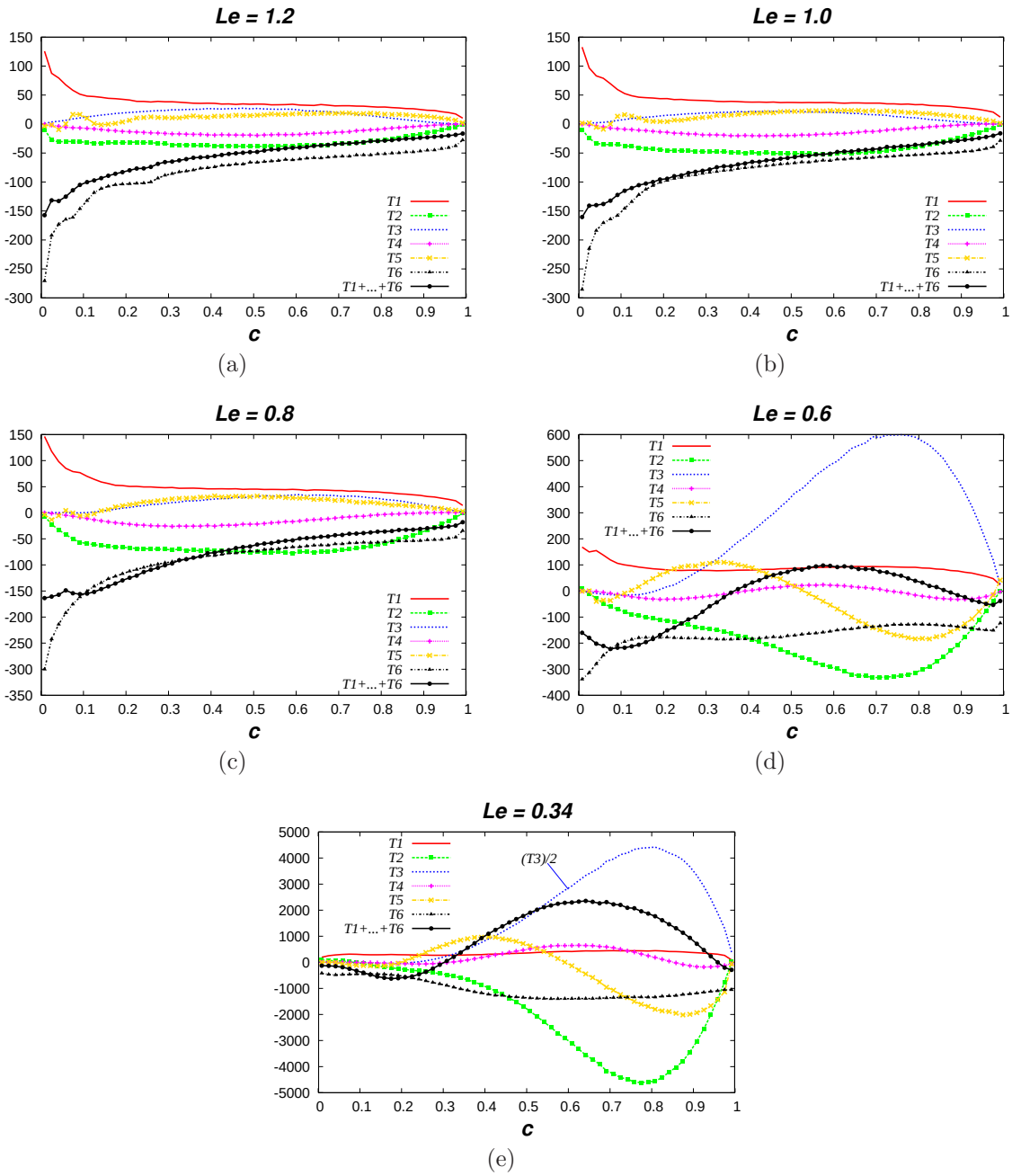

FIG. 4: Mean values of the various terms in the enstrophy conservation equation (9), conditional upon c. (a) $Le = 1.2$, (b) $Le = 1.0$, (c) $Le = 0.8$, (d) $Le = 0.6$, and (e) $Le = 0.34$. Variables have been normalized with $(\delta_{th}/S_L)^3$ corresponding to the $Le = 1.0$ flame. The mean value of T_3 for $Le = 0.34$ has been divided by two.

To understand the causes of the previous behavior, the mean values of the different terms in the enstrophy transport equation, conditional on the value of c, for different Lewis numbers are shown in Figure 4. At a given instant, these terms do not necessarily balance and the imbalances of contributions to the right side of Eq. (5) (i.e., the left side or material derivative of the enstrophy of a fluid particle) are plotted for the various cases. An overall destruction of enstrophy is apparent across the flame for Le equal to 0.8, 1.0 and 1.2, while there is a moderate (high) generation of enstrophy within the flame for $Le = 0.6$ ($Le = 0.34$).

For the $Le = 0.8, 1.0$ and 1.2 cases the different terms display similar trends; vortex-stretching and viscous dissipation are the dominant mechanisms towards the unburned gas side of the flame front. Within the flame all terms display a comparable contribution to enstrophy generation. Moreover, the mean value of viscous transport of enstrophy conditional on c in these cases is not negligible compared to the mean viscous dissipation. On the other hand, annihilation/generation by volumetric dilatation rates is negative as a consequence of heat release by the flame, nearly vanishes at the extreme values of c and becomes more important as the Lewis number decreases, due to grater extent of burning with decreasing Le. The baroclinic torque exhibits a positive contribution to the enstrophy transport over most values of c, with a maximum within the preheat zone, almost vanishing at $c = 0$ and $c = 1$ and slightly increasing as Le decreases. The viscous torque has a small, though not negligible, contribution for the cases considered here.

It can also be seen in Figure 4 that the baroclinic torque plays a particularly important role for the $Le = 0.34$ and $Le = 0.60$ cases, and exhibits very large maxima near the most reactive region within the flame; small negative values towards the unburned gas give way to large positive values for the major part of the rest of the flame front. Vortex-stretching and viscous dissipation for $Le = 0.6$ show similar trends to those for the cases with $Le \geq 0.8$, and assume comparable values; for $Le = 0.34$ vortex-stretching is approximately constant for all values of c, whereas viscous dissipation takes small values in the fresh reactants, which increase within the flame due, among other cause, to the increment of the kinematic viscosity. The behavior of the viscous diffusive transport of enstrophy for $Le = 0.34$ and Le = 0.6 is rather different from that at larger Lewis numbers; it changes within the flame from positive values to negative ones around the middle of the flame and the magnitude of mean viscous transport becomes greater than mean viscous dissipation around the maximum values of the chemical conversion rate. The mean viscous torque contribution is smaller than

the remaining terms throughout all values of c for $Le = 0.6$, but it becomes comparable to the mean contribution of the vortex-stretching term for $Le = 0.34$. Enstrophy annihilation by volumetric dilatation rates, due to a large heat release rate, becomes a leading sink and dominates over the viscous dissipation for a significant portion of the composition domain ($c > 0.4$). The enstrophy generation induced by the baroclinic torque is partially countered by the remaining five terms.

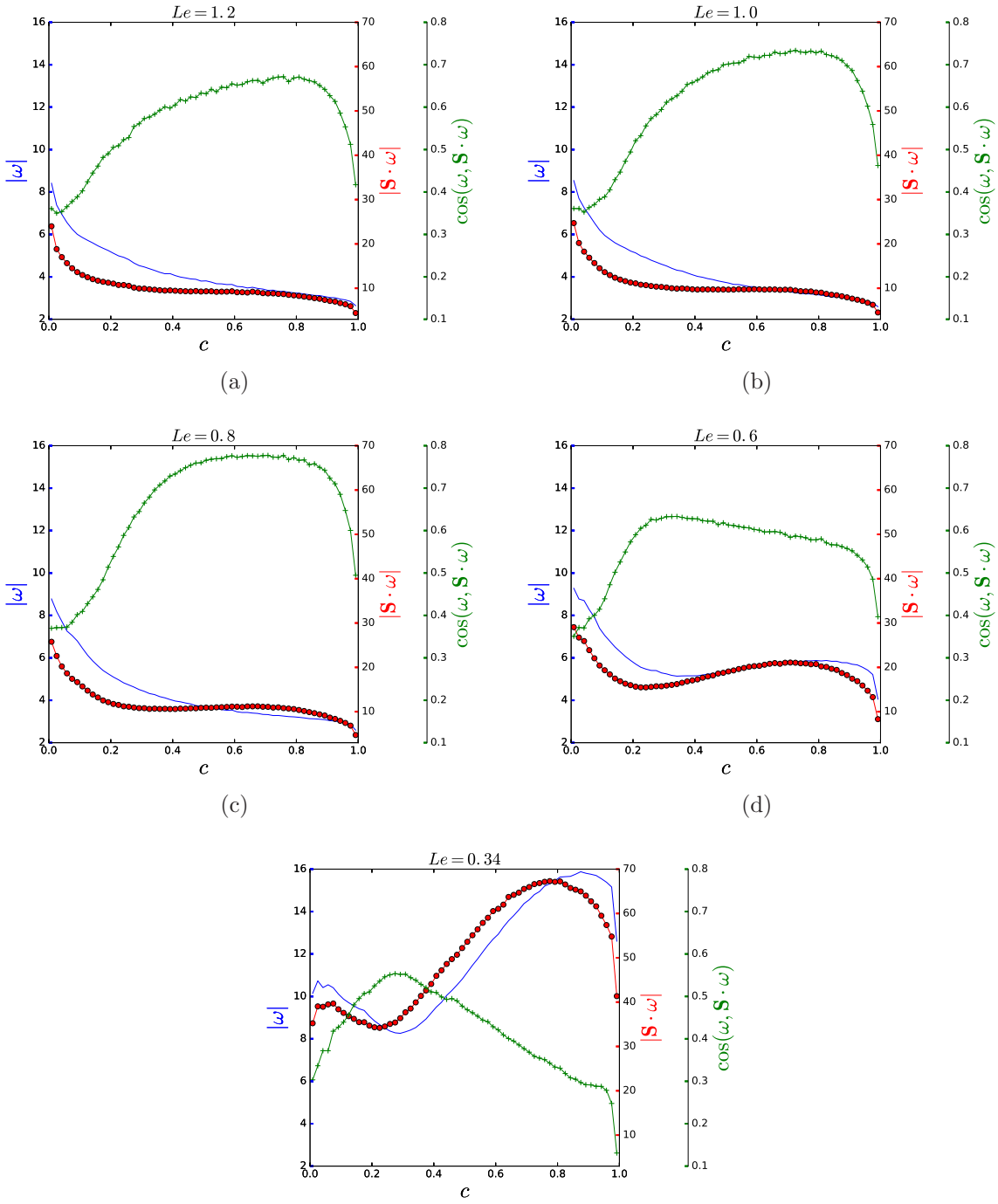

FIG. 5: Mean values of vorticity, $|\boldsymbol{\omega}|$, and vortex-stretching, $|\mathbf{S}\cdot\boldsymbol{\omega}|$, magnitudes and of $\cos(\boldsymbol{\omega}, \mathbf{S}\cdot\boldsymbol{\omega})$, conditional upon c. (a) $Le = 1.2$, (b) $Le = 1.0$, (c) $Le = 0.8$, (d) $Le = 0.6$ and (e) $Le = 0.34$. $\boldsymbol{\omega}$ and $(\mathbf{S}\cdot\boldsymbol{\omega})$ have been normalized with (δ_{th}/S_L) and $(\delta_{th}/S_L)^2$, respectively, corresponding to the $Le = 1.0$ flame.

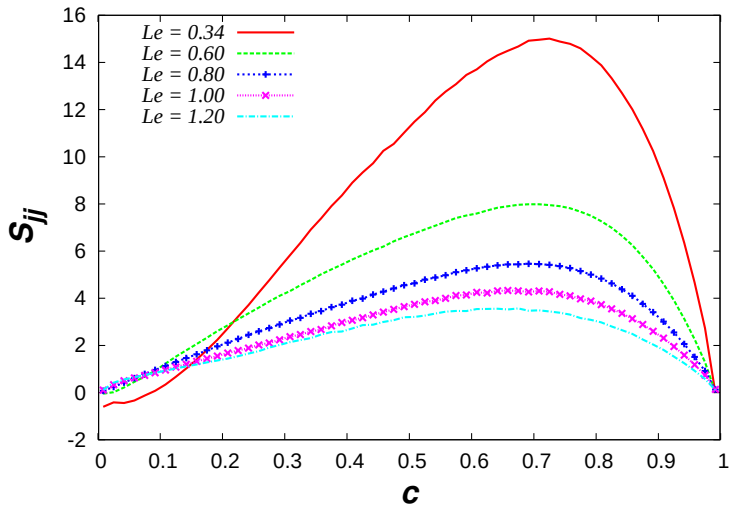

FIG. 6: Volumetric Dilatation rate, S_{jj}, conditional upon c, at different Le. S_{jj} has been normalized with (δ_{th}/S_L) corresponding to the $Le = 1.0$ flame.

The magnitudes of the vorticity, $\boldsymbol{\omega}$, and the vortex-stretching, $\mathbf{S}\cdot\boldsymbol{\omega}$, and the cosine of the angle of these two vectors are shown in Figure 5. The alignment vorticity/vortex-stretching lessens as flames become more convoluted for decreasing Lewis numbers. The variations of the three magnitudes across the flame explain the patterns of T_1 depicted in Figure 4 for different values of Le. The positive volumetric dilatation rate due to heat release, shown in Figure 6, implies that term T_2 is a sink of enstrophy over all values of c, consistent with features of Figure 4; the annihilation rate is more pronounced for lower Lewis numbers, due to more intense heat release rates. The variation of $|\boldsymbol{\omega}|$ is consistent with the variation of E shown in Figure 3. The augmentation of burning rate with decreasing Le gives rise to stronger thermal expansion effects for flames with smaller value of Le. This can be substantiated from the mean values of $S_{jj} = \nabla\cdot\mathbf{u}$ conditional on c shown in Fig. 6, which reveals an increase in the magnitude of S_{jj} with decreasing Le. Strong flame normal acceleration and high extent of flame wrinkling contribute to an increase in the magnitude of strain rates with decreasing Le. This is reflected in the increases in the magnitude of $|\mathbf{S}\cdot\boldsymbol{\omega}|$ with decreasing Lewis number Le. The vortex-stretching term T_1 can be rewritten as $T_1 = \boldsymbol{\omega}\cdot(\mathbf{S}\cdot\boldsymbol{\omega}) = |\boldsymbol{\omega}||\mathbf{S}\cdot\boldsymbol{\omega}|\cos(\boldsymbol{\omega},(\mathbf{S}\cdot\boldsymbol{\omega})) = 2(\mathbf{e}_\alpha\cos^2\alpha + \mathbf{e}_\beta\cos^2\beta + \mathbf{e}_\gamma\cos^2\gamma)E$, where $\mathbf{e}_\alpha$, $\mathbf{e}_\beta$ and $\mathbf{e}_\gamma$ are the most extensive, intermediate and the most compressive principal strain rates respectively, and the angles between $\boldsymbol{\omega}$ and the eigenvectors associated with $\mathbf{e}_\alpha$, $\mathbf{e}_\beta$ and $\mathbf{e}_\gamma$ are given by α, β and γ respectively. It has been shown by Chakraborty [31] that $\boldsymbol{\omega}$ predominantly aligns with $\mathbf{e}_\beta$ (i.e. $|\cos\beta| \approx 1$) but the extent of alignment with $\mathbf{e}_\alpha$ increases

in the regions of high chemical heat release for $Le \approx 1.0$ cases. The extent of $\boldsymbol{\omega}$ alignment with $\mathbf{e}_\alpha$ ($\mathbf{e}_\gamma$) decreases (increases) with decreasing Lewis number [31] and interested readers are referred to [31] for relevant explanations. The probability of increased alignment with the most compressive (i.e. most negative) principal strain rate is responsible for the reduction of the mean value of $\cos(\boldsymbol{\omega}, (\mathbf{S}\cdot\boldsymbol{\omega}))$ with decreasing Le.

The term T_3, the baroclinic torque contribution to E in equation (5), can be expressed as:

$$\begin{aligned}\frac{1}{\rho^2}\boldsymbol{\omega}\cdot[(\nabla\rho)\times(\nabla p)] &= \frac{1}{\rho^2}|\boldsymbol{\omega}||(\nabla\rho)\times(\nabla p)|\cos(\boldsymbol{\omega}, \nabla\rho\times\nabla p)\\ &= \frac{1}{\rho^2}|\boldsymbol{\omega}||\nabla\rho||\nabla p||\sin(\nabla\rho,\nabla p)|\cos(\boldsymbol{\omega},\nabla\rho\times\nabla p)\,. \end{aligned} \tag{18}$$

The sizable growth of enstrophy with the reaction progress variable for the $Le = 0.34$ and 0.6 cases can be explained in terms of the variations of $|\boldsymbol{\omega}|$, $|\nabla\rho|$ and $|\nabla p|$ and the corresponding alignments given by $\cos(\boldsymbol{\omega}, \nabla\rho\times\nabla p)$ and $|\sin(\nabla\rho,\nabla p)|$. The sign of $\cos(\boldsymbol{\omega}, \nabla\rho\times\nabla p)$ determines whether T_3 is a source or a sink of E. Figure 7 depicts the mean value of $\cos(\boldsymbol{\omega}, \nabla\rho\times\nabla p)$ as a function of c for different Lewis numbers. Enstrophy is generated within the flame ($0.30 < c < 0.95$) by the baroclinic torque for all cases considered here. Some destruction of enstrophy can only occur in part of the fresh reactants for the $Le = 0.34, 0.6$ and 0.8 cases and in the hot products for the $Le = 1.0$ and 1.2 cases. The values of $\cos(\boldsymbol{\omega}, \nabla\rho\times\nabla p)$ are relatively small (less than 0.3) for the $Le = 0.8, 1.0$ and 1.2 cases and significantly higher (between 0.3 and 0.9) for the $Le = 0.34$ and 0.6 cases. Therefore, the alignment of $\boldsymbol{\omega}$ and $[(\nabla\rho)\times(\nabla p)]/\rho^2$ changes appreciably with Le.

The variation of the mean value of $|\boldsymbol{\omega}|$ with c is similar to that in Figure 3 for the enstrophy. Figure 8 shows the mean values of $|\nabla\rho|$ and $|\nabla p|$, conditional upon c for different Lewis numbers. The values of $|\nabla\rho|$ and $|\nabla p|$ within the flame for $Le = 0.34$ and $Le = 0.6$ are considerably higher than those for the $Le = 0.8, 1.0$ and 1.2 cases.

Weakening of thermal diffusion rate with decreasing Le increases the probability of finding high values of $|\nabla T_{ins}|$ [38, 45], which gives rise to an increase of the mean values of $|\nabla\rho| = \rho^2\tau|\nabla T_{ins}|/[\rho_u(T_{ad}-T_u)]$ with decreasing Le. Furthermore, higher rate of burning for smaller values of Le gives rise to stronger flame normal acceleration. This strengthening of flame normal acceleration with decreasing Le is reflected in the increasing trend of mean values of

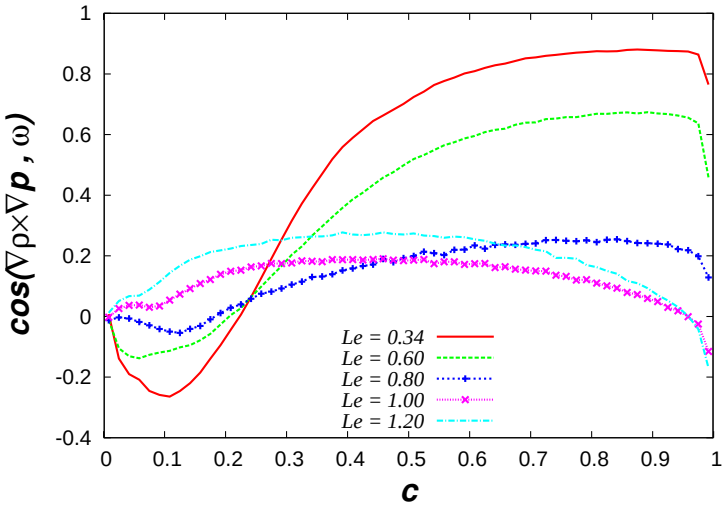

FIG. 7: Mean value of $\cos(\nabla\rho \times \nabla p, \boldsymbol{\omega})$ conditional upon c for different Lewis numbers.

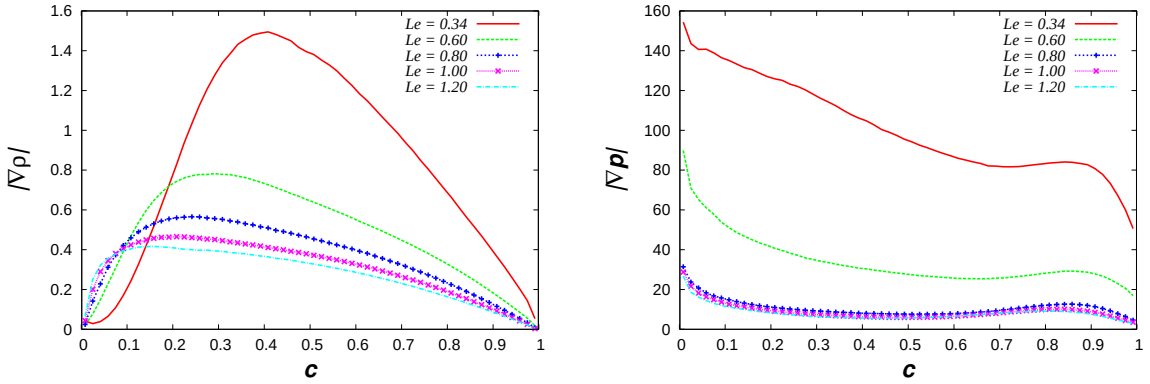

(a) (b)

FIG. 8: Mean modulus of the (a) density gradient, $|\nabla\rho|$, and (b) pressure gradient, $|\nabla p|$ conditional upon c for different Lewis numbers. $|\nabla\rho|$ and $|\nabla p|$ have been normalized by (δ_{th}/ρ_u) and $\left[\delta_{th}/(\rho_u S_L^2)\right]$ of the unity Lewis number flame, respectively.

$|\nabla p|$ with a decrease in global Lewis number. Interested readers are referred to Refs. [45, 58] for more detailed discussion on the effects of Le on both scalar and pressure gradients.

Figure 9 depicts the mean values of $|\sin(\nabla\rho, \nabla p)|$, conditional upon c for different Lewis numbers; these values, particularly in the burning region, for the $Le = 0.34$ and $Le = 0.6$ are considerably higher than the corresponding ones for the $Le = 0.8, 1.0$ and 1.2 cases.

Magnitudes of $|\boldsymbol{\omega}|$, $|\nabla\rho|$, $|\nabla p|$, $|\sin(\nabla\rho, \nabla p)|$, and $|\cos(\nabla\rho \times \nabla p, \boldsymbol{\omega})|$, for $Le < 0.8$ cases and $c > 0.3$, are considerably higher than those for $Le \geq 0.8$. This implies that an increase of the baroclinic torque contribution to E in the regions with high chemical activities and this trend is particularly strong for low Lewis numbers. The latter is apparent in Figure 10

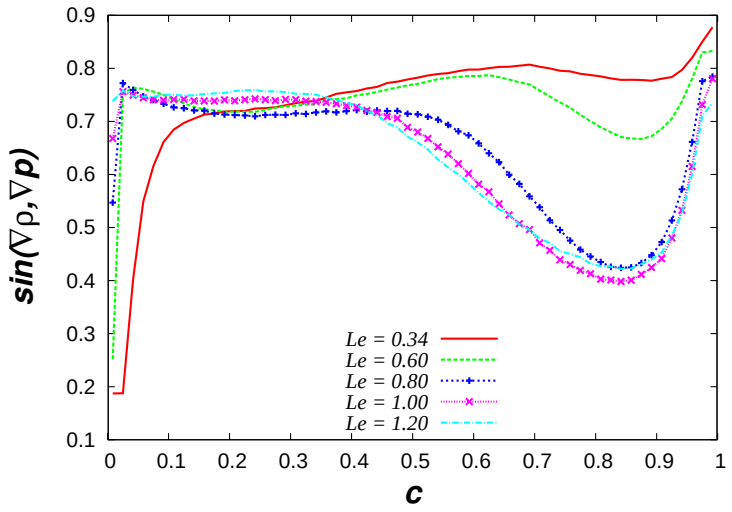

FIG. 9: Mean value of $|\sin(\nabla\rho, \nabla p)|$ conditional upon c for different Lewis numbers.

for the mean value of $T_3 = \boldsymbol{\omega} \cdot [(\nabla\rho) \times (\nabla p)] / \rho^2$ for the various Lewis numbers; T_3 increases considerably from the preheat region to hot products for $Le = 0.34$ and, to a lesser extent, for $Le = 0.60$. It has been already pointed out that T_3 becomes the most important contribution to E for low Lewis number cases (see Figure 4). Further characterization and additional details to the previous description are provided in Figure 11, which depicts the alignments of vectors $\boldsymbol{\omega}$, $\nabla\rho$, ∇p and ∇T_{ins} with the unit vector normal to the iso-scalar surfaces, $\mathbf{n} = -\nabla c/|\nabla c|$. It is evident that $\nabla\rho$ and ∇T_{ins} are apparently aligned and counter-aligned, respectively, with $\mathbf{n}$, and are therefore, almost normal to the flame (see Figures 11(a) and 11(b)). The vorticity vector, $\boldsymbol{\omega}$, seems to be predominantly orthogonal to $\mathbf{n}$ within the flame for all Lewis numbers (Figure 11(c)). The vectors ∇p and $\mathbf{n}$ show no preferred relative orientation (Figure 11(d)); The mean alignments of $\mathbf{n}$ and $\boldsymbol{\omega}$ with respect to the eigenvectors of the strain rate tensor have been discussed elsewhere [38].

For low Mach number and unity Lewis number flames, the non-dimensional temperature $T = (T_{ins} - T_0)/(T_{ad} - T_0)$ can be equated to c and $\nabla\rho$ can be expressed as $\nabla\rho \approx \tau\rho^2|\nabla c|\mathbf{n}/\rho_0$, which leads to $\partial\rho/\partial x_N = \mathbf{n} \cdot \nabla\rho \approx -\rho\mathbf{n} \cdot \nabla T/T = \tau\rho^2|\nabla c|/\rho_0$. It was demonstrated by Chakraborty et al. [38] that $\overline{|\nabla\rho|} \approx \overline{(\partial\rho/\partial x_N)}$ because $(-\mathbf{n} \cdot \nabla T)$ remains close to $|\nabla c|$ even for $Le \neq 1.0$ flames. This suggests that $\rho^{-2}\nabla\rho \times \nabla p$ can be approximated as $\rho^{-2}\nabla\rho \times \nabla p \sim \tau|\nabla c|\mathbf{n} \times \nabla p/\rho_0$, which indicates that only the pressure gradient in the tangential direction to the flame $(\partial p/\partial x_i)_t = (\delta_{ij} - n_i n_j)\partial p/\partial x_j$ contributes to the baroclinic torque. It is worth noting that $\overline{|(\nabla p)_N|)} = |\mathbf{n} \cdot \nabla p|$ is related to the flame normal acceleration, while

the local pressure gradient in the tangential direction is induced by the surrounding flame wrinkles. The extent of flame wrinkling increases with decreasing Le. The combination of high magnitudes of $(\nabla p)_t$ and $\nabla\rho$ in the $Le < 0.8$ flames gives rise to high values of $\rho^{-2}\nabla\rho \times \nabla p$. The directions between $\boldsymbol{\omega}$ and $\rho^{-2}\nabla\rho \times \nabla p$ are independent of each other for both leading and trailing edges of the flame brush for the $Le = 0.6$, 0.8, 1.0 and 1.2 flames. Although directions of $\boldsymbol{\omega}$ and $\rho^{-2}\nabla\rho \times \nabla p$ remain completely independent of each other for the leading edge of the flame brush, they are related on the burned gas side in the $Le = 0.34$ flame due to significant density variation.

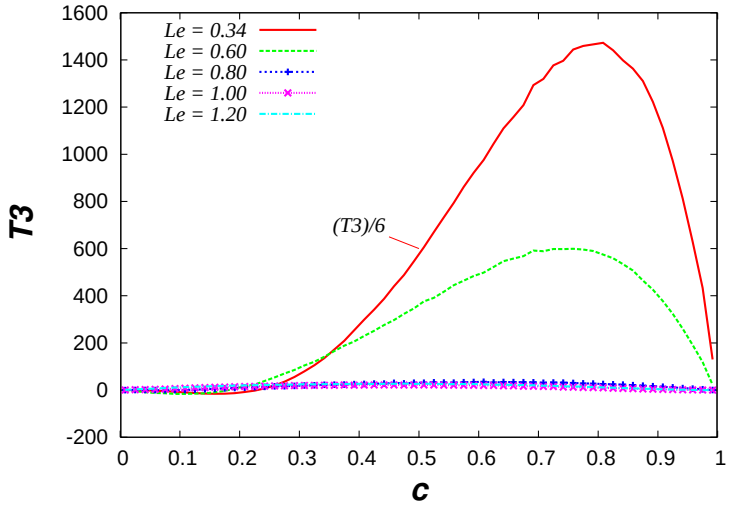

FIG. 10: Mean baroclinic torque contribution to enstrophy generation, T_3, conditional upon c, for different Lewis numbers. T_3 has been normalized by $(\delta_{th}/S_L)^3$ of the unity Lewis number flame. The mean value of T_3 for $Le = 0.34$ has been divided by six.

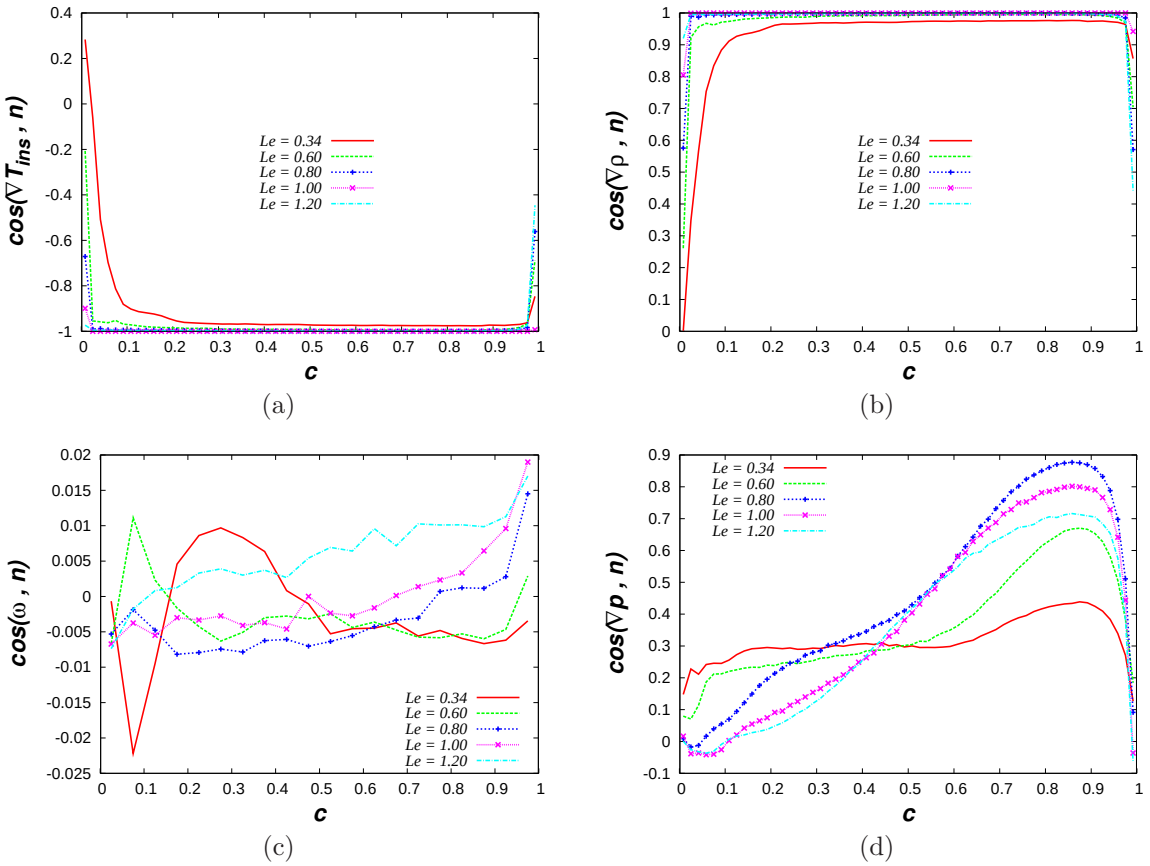

FIG. 11: Mean alignments of the unit vector, $\mathbf{n}$, normal to the iso-scalar surface $c(\mathbf{x}, t) = const$ and (a) temperature gradient, (b) density gradient, (c) vorticity vector, and (d) pressure gradient.

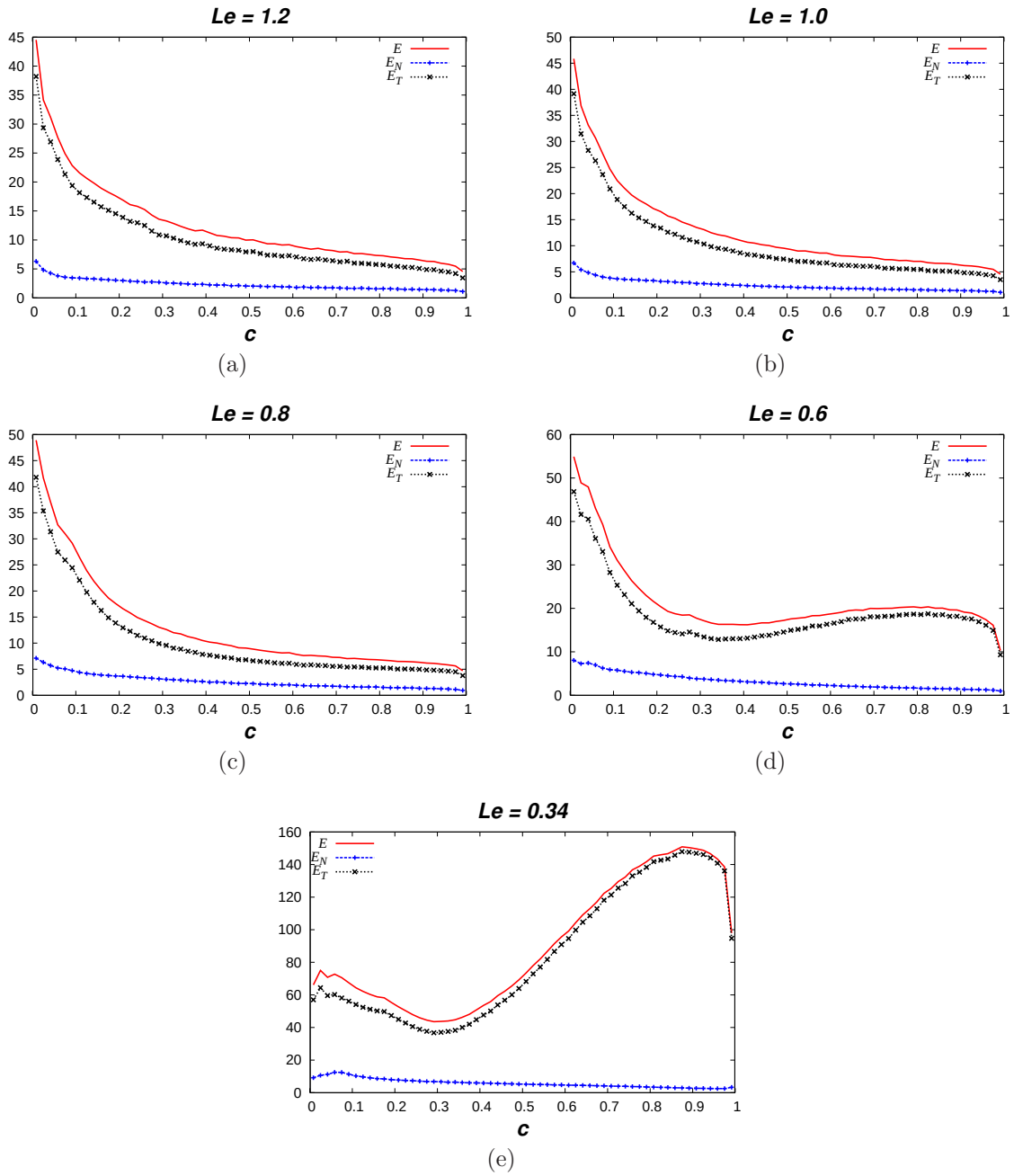

FIG. 12: Mean values of the enstrophies of the vorticity vector components tangential and normal to iso-scalar surfaces, conditional upon c, at different Le. (a) $Le = 1.2$, (b) $Le = 1.0$, (c) $Le = 0.8$, (d) $Le = 0.6$, and (e) $Le = 0.34$. Variables have been normalized with $(\delta_{th}/S_L)^2$ corresponding to the $Le = 1.0$ flame.

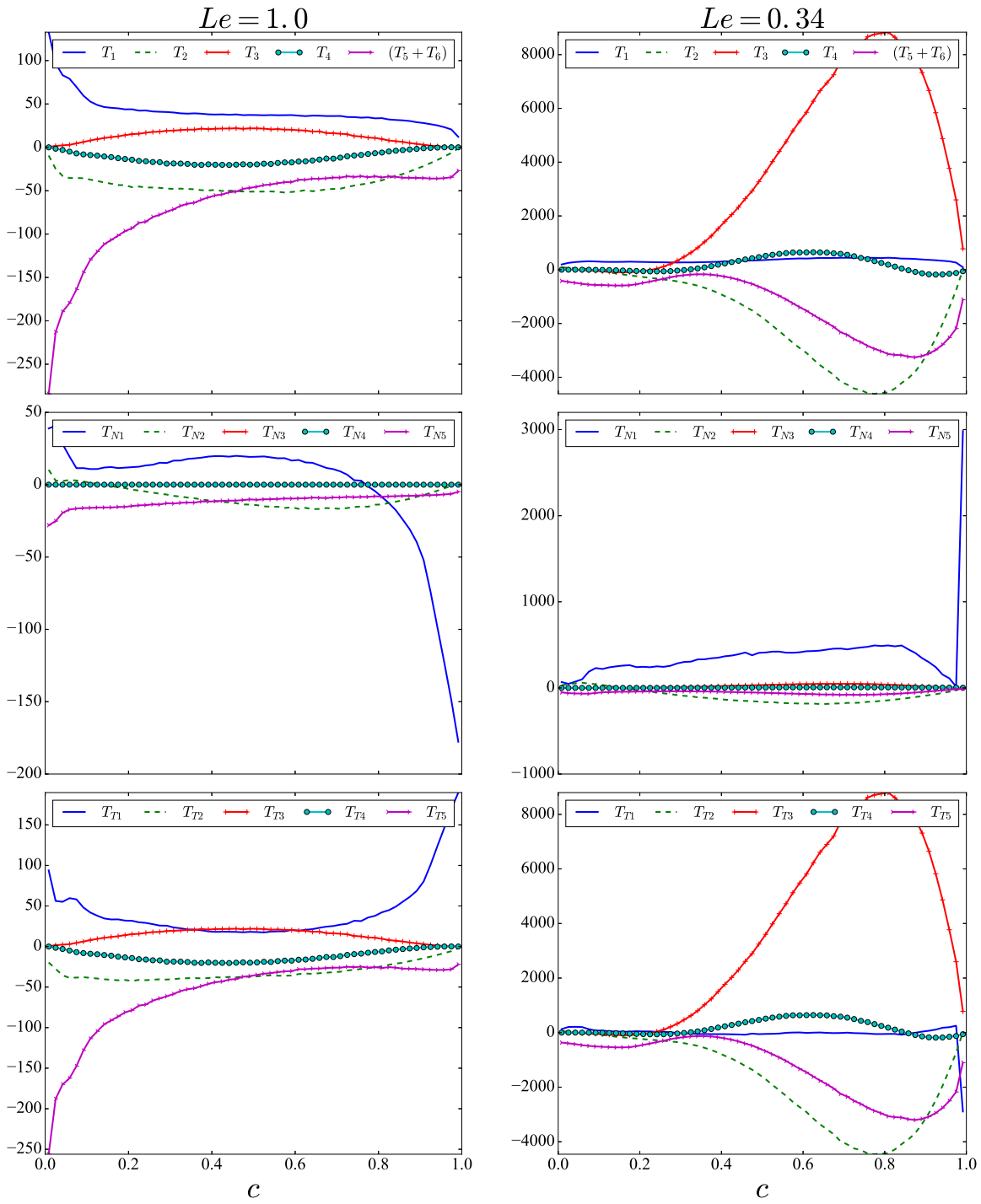

FIG. 13: Mean values of the various terms of the enstrophy and the enstrophies of the vorticity vector components tangential and normal to iso-scalar surfaces, conditional upon c. (a) $Le = 1.0$ and (b) $Le = 0.34$. Variables have been normalized with $(\delta_{th}/S_L)^3$ corresponding to the $Le = 1.0$ flame.

Furthermore, the relative orientation of $\rho(\mathbf{x},t) = const$ and $p(\mathbf{x},t) = const$ iso-surfaces, or, equivalently, the alignment of $\nabla\rho$ and ∇p, determine the magnitude of $|\sin(\nabla\rho \times \nabla p)|$. Since ∇p is given by the momentum equation and $\nabla\rho \approx |\nabla\rho|\mathbf{n}$, the baroclinic plus viscous torques can be recast as

$$-\frac{1}{\rho^2}\nabla\rho \times (-\nabla p + \nabla\cdot\tau) \approx -\frac{1}{\rho}|\nabla\rho|\mathbf{n} \times \frac{D\mathbf{u}}{Dt}\,. \tag{19}$$

Therefore, the local fluid particle acceleration in the tangential direction to the flame, dictate the baroclinic plus viscous torques. Fluid acceleration within the flame tends to moderately align with the inflow-outflow direction for Le equal to 0.34 and 0.6, whereas $\mathbf{n}$ deviates from that orientation as Le decreases, due to flame rotation, twisting and folding. The magnitude of the right side will thus increase as Le reduces. Moreover, the baroclinic source (T_3) and the viscous torque sink (T_4) tend to balance each other for Le equal to the 0.8, 1.0 and 1.2 cases (Figure 4). In any event, the viscous force torque remains a minor contributor to enstrophy production or destruction for all Lewis numbers.

The quantity $\cos(\boldsymbol{\omega},\mathbf{n})$ is expected not to vary much; Chakraborty [31] demonstrated that vorticity shows significant alignment with the eigenvector of the intermediate principal strain rate for all cases, whereas it considerably aligns with the eigenvector of the most compressive principal strain rate for the $Le = 0.34$ case, this tendency increasing with decreasing Lewis number. The flame normal aligns predominantly with the eigenvector of the most extensive principal strain rate in these flames [38]. Due to the orthogonality of the eigenvectors of the principal strain rates, $\cos(\boldsymbol{\omega},\mathbf{n})$ may not show much variation across the flame, which does not mean that the qualitative nature of the vorticity alignment with these local eigenvectors does not change with the Lewis number.

The analysis in this study is conducted for a single set of values of u'/S_L and τ, for different values of Le (0.34, 0.6, 0.8, 1.0 to 1.2). For the values of u'/S_L and τ used here, significant enstrophy production takes place for $Le = 0.34$ and 0.6 flames due to strong baroclinic vorticity generation mechanisms, whereas that contribution is relatively weak in comparison to the molecular dissipation of enstrophy for $Le = 0.8$, 1.0 and 1.2 cases. A modification of either u'/S_L or τ will modify the threshold Lewis number for which flame-induced enstrophy generation will be observed, while the strengthening of the baroclinic torque will continue to happen with decreasing Le.

An analysis of enstrophies of the vorticity vector components tangential and normal to iso-scalar surfaces offers an alternative perspective. Figure 12 shows that a sizable fraction of the total enstrophy is ascribable to the vorticity component tangential to iso-surfaces for all Lewis numbers and all regions of the flame. This confirms previous findings [32] that the vorticity vector is predominantly tangent to iso-scalar surfaces. Moreover, Figure 13 illustrates for $Le = 1.0$ and $Le = 0.34$ the contributions to E_T and E_N of vortex-stretching, volumetric dilatation rates, baroclinic and viscous force torques and combined viscous transport plus dissipation. Contributions to E_T are obtained by subtracting the corresponding terms in the transport equation for E_N from these in the transport equation for E. For $Le = 1.0$ (and seemingly for $Le = 0.8$ and $Le = 1.2$) the vortex-stretching term is a source of E_T within the flame, increasing toward the trailing edge, whereas it contributes positively (negatively) to E_N towards the unburned (burned) gas side of the flame front; vortex-stretching is the leading order contributor to E_N, but it is negligible in the E_T transport budget. Both trends can be explained from the magnitudes of the vectors $\boldsymbol{\omega}$ and $\mathbf{S}\cdot\boldsymbol{\omega}$, and alignments shown in Figures 5 and 11. Annihilation by volumetric dilatation rates for $Le = 1.0$ has small negative contributions to both E_T and E_N, while it is an major (minor) sink of E_T (E_N) for $Le = 0.34$; Figure 6 and expressions for the annihilation terms of E_N, $-2(S_{jj} + a_N)E_N$ and E_T, $-2S_{jj}E_T + 2a_N E_N$, where the normal strain rate, $a_N > 0$, help to clarify these results. Apparently, the baroclinic torque only generates E_T; this seems obvious from the previous remarks on the predominant alignment of $\nabla\rho$ and $\mathbf{n}$, which implies that the baroclinic torque contribution to E_N in Eq. (9) is almost zero. The source of E_T due to the baroclinic torque is moderate for $Le = 1.0$ and extremely high for $Le = 0.34$. For the two Lewis numbers the viscous force torque contributes negligibly to E_N, and acts as a small sink (source) of E_T for $Le = 1.0$ ($Le = 0.34$) within most of the flame. The combined viscous transport plus dissipation displays a small negative contribution of E_N, whereas it becomes a leading order sink in the E_T transport.

On the other hand, for $Le = 0.34$ (and also for $Le = 0.6$) vortex-stretching leads contributions to E_N and is negligible for E_T. Annihilation by volumetric dilatation displays a small contribution to E_N and a large one for E_T, more pronounced in the flame zone due to heat release, and the generation of E_N by the baroclinic torque is negligible and becomes the leading term for E_T (for the same reasons explained for $Le \geq 0.8$). Viscous force torque productions of E_T and E_N are both negligible. The combined negative contributions to E_N

and E_T of viscous transport and dissipation are comparable for $Le = 1.0$; for $Le = 0.34$ it is a leading sink of E_T, causing only small destruction of E_N.

V. CONCLUSIONS

A transport equation for the enstrophy, E, of a variable-density flow of a constant dynamic viscosity fluid has been derived. An analogous equation for the enstrophy of the vorticity component normal to a given iso-scalar surface (within a flame), E_N, has also been obtained. The term by term difference between the former and the latter transport equations yields the various sources and sinks contributing to the enstrophy of the vorticity component tangential to an iso-surface, E_T. Decomposing the vorticity into its components normal and tangential to the flame clarifies the relative importance of contributions to E across the flame.

The global Lewis number, Le, has been shown to have a profound influence on the evolution of the enstrophy field within turbulent premixed statistically planar flames. Examination of an existing DNS dataset shows that the enstrophy is significantly destroyed across the flame for Le equal to 0.80, 1.00 and 1.20. On the contrary, for $Le = 0.60$ a slight augmentation of the enstrophy is observed within the flame, where a remarkable growth of enstrophy is apparent for $Le = 0.34$.

The various terms in the enstrophy transport equation have been computed across the flame for different Lewis numbers. Vortex-stretching and viscous dissipation are the leading order contributors for the cases with Lewis numbers equal to 0.80, 1.0 and 1.20, whereas the remaining mean contributions are slightly smaller although comparable. By contrast, for the cases with Lewis numbers equal to 0.60 and 0.34 the mean contribution of baroclinic torque is significantly greater than the other mean contributions within the flame; the mean contributions of vortex-stretching, destruction by volumetric dilatation rates and viscous transport and dissipation remain comparable over most of the flame. The viscous torque is relatively small.

The variation with Le of mean magnitudes of $\boldsymbol{\omega}$ and $\mathbf{S}\cdot\boldsymbol{\omega}$, and of their alignment across the flame explain the behavior of the source of enstrophy by vortex-stretching. The mean value of the volumetric dilatation rate, conditional upon the reaction progress variable, account for changes in the enstrophy annihilation for different Lewis numbers.

An explanation for the qualitative and quantitative differences in the baroclinic torque

contribution, T_3, to the enstrophy transport equation, which occurs between $Le = 0.6$ and $Le = 0.8$, is sought in terms of the alignments of vorticity and the gradients of density and pressure, as well as their corresponding magnitudes. Positive values of $\cos(\boldsymbol{\omega}, \nabla\rho \times \nabla p)$ within the flame indicate that enstrophy is always generated for all cases considered here; however, the strength of T_3 increases for $Le = 0.6$ and most notably for $Le = 0.34$, due to consistently higher individual values of $|\boldsymbol{\omega}|$, $|\nabla\rho|$, $|\nabla p|$, $\sin(\nabla\rho, \nabla p)$, and $\cos(\boldsymbol{\omega}, \nabla\rho \times \nabla p)$. It is found that $\nabla\rho$ is almost perfectly aligned with $\mathbf{n}$, the unit vector normal iso-scalar surfaces within the flame. The pressure gradient tangential to the flame, or, equivalently, the tangential acceleration to it, is thus responsible for the high magnitude of the baroclinic torque, which increase as Le decreases due to high chemical heat release, low heat conduction and significant flame wrinkling triggered by the diffusive-thermal instability.

The vorticity vector component tangential to iso-scalar surfaces is shown to be by far the major contributor to the total enstrophy. Budgets of the right sides of the enstrophy transport equations for E_T and E_N show that, while for $Le = 1.0$ vortex-stretching, destruction by volumetric dilatation and the combination of viscous transport and dissipation are the main contributors to E_N, all the terms are comparable within the flame for the E_T balance. On the other hand, for $Le = 0.34$, vortex stretching and annihilation by dilatation are leading contributions to E_N, whereas the baroclinic torque, annihilation by dilatation and combined viscous transport and dissipation determine the evolution of E_T.

Acknowledgments

C.D. and L.C. gratefully acknowledge the support of this research by the Spanish Ministry of Economy and Competitiveness, under the CONSOLIDER-INGENIO Program, Project CS D2010-00011-SCORE. N.C. acknowledges N8/ARCHER for computational resources. L.C. acknowledges the funding of the Marie Sklodowska-Curie Actions from the European Commission H2020-MSCA-IF-2015-EF under the EU-Project 706672 - ITPF.

[1] H. Tennekes and J. Lumley, MIT Press (1972).

[2] A. Chorin, Applied Mathematical Sciences, Springer-Verlag **103** (1994).

[3] B. Karlovitz, D. Denniston, and F. Wells, J. Chem. Phys. **19**, 541 (1951).

[4] A. Eschenroeder, Phys. Fluids **7**, 1735 (1964).

[5] R. Günther and B. Lenze, 14th Symp. (International) on Combcaust. **14**, 675 (1973).

[6] D. Ballal, Proc. Royal Soc. **London A367**, 353 (1979).

[7] J. Driscoll and A. Gulati, Combust. Flame **72**, 131 (1988).

[8] S. Pope, Ann. Rev Fluid Mech. **19**, 237 (1987).

[9] N. Chakraborty, M. Katragadda, and R. Cant, Phys. Fluids **23**, 075109 (2011).

[10] N. Chakraborty, M. Katragadda, and R. Cant, J. Flow Turb. Combust. **87**, 205–235 (2011).

[11] A. Steinberg, J. Driscoll, and S. Ceccio, Exp. Fluids **44**, 985 (2008).

[12] A. Steinberg and D. J.F., Combust. Flame **156**, 2285 (2009).

[13] A. Steinberg, J. Driscoll, and S. Ceccio, Exp. Fluids **47**, 527 (2009).

[14] Y.-H. Im, K. Huh, S. Nishiki, and T. Hasegawa, Combust. Flame **137**, 478 (2004).

[15] K. Nomura and S. Elghobashi, Theor. Fluid Dyn. **5**, 153 (1993).

[16] O. Boratav, S. Elghobashi, and R. Zhong, Phys. Fluids **10(9)**, 2260 (1996).

[17] S. Elgobashi, R. Zhong, and O. Boratav, Phys. Fluids **11(10)**, 3123 (1999).

[18] F. Jaberi, D. Livescu, and C. Madnia, Phys. Fluids **12(5)**, 1189 (2000).

[19] D. Louch and K. Bray, Combust. Flame **125**, 1279–1309 (2001).

[20] G. JaberiPatnaik and K. Kailasanath, NASA/CP-2003-212376/REV1 pp. 225–228 (2003).

[21] S. Shanbhogue, S. Husain, and T. Lieuwen, Progress Energy Combust. Sci. **35**, 98 (2009).

[22] Z. Carr and D. Forliti, 48th AIAA Aerospace Sci Meet. Orlando (2010).

[23] A. Lipatnikov, S. Nishiki, and T. Hasegawa, Phys. Fluids **26**, 105104 (2014).

[24] A. Lipatnikov and J. Chomiak, Progress Energ. Combust. Sci. **36**, 1 (2010).

[25] P. Hamlington, A. Poludnenko, and E. Oran, Phys. Fluids **23**, 125111 (2011).

[26] T. Treurniet, F. Nieuwstadt, and B. Boersma, J. Fluid Mech. **565**, 25 (2006).

[27] L. Cifuentes, Ph.D. Dissertation, University of Zaragoza (2015).

[28] L. Cifuentes, C. Dopazo, J. Martin, and C. Jimenez, Phys. Fluids **26**, 065108 (2014).

[29] D. Haworth and T. Poinsot, J. Fluid Mech. **244**, 405–436 (1992).

[30] C. Rutland and A. Trouvé, Combust. Flame **94**, 41–57 (1993).

[31] N. Chakraborty, European J. Mechanics B/Fluids **46**, 201 (2014).

[32] N. Chakraborty, I. Konstantinou, and A. Lipatnikov, Phys. Fluids **28**, 015109 (2016).

[33] J. J. Gorski and P. S. Bernard, International journal of engineering science **34**, 699 (1996).

[34] B. Bobbitt, S. Lapointe, and G. Blanquart, Physics of Fluids **28**, 015101 (2016).

[35] B. Bobbitt and G. Blanquart, Physics of Fluids **28**, 105101 (2016).

[36] R. Ranjan, B. Muralidharan, Y. Nagaoka, and S. Menon, Combustion Science and Technology **188**, 1496 (2016).

[37] K. Jenkins and R. Cant, The Combustion Institute **2**, 192 (1999).

[38] N. Chakraborty, M. Klein, and N. Swaminathan, Proc. Combust. Inst. **32**, 1409 (2009).

[39] N. Chakraborty and R. Cant, Combust. Flame **158**, 1768–1787 (2011).

[40] W. T. Ashurst, N. Peters, and M. Smooke, Combustion science and technology **53**, 339 (1987).

[41] A. Trouvé and T. Poinsot, Journal of Fluid Mechanics **278**, 1 (1994).

[42] I. Han and K. Huh, Combust. Flame **152**, 194–205 (2008).

[43] N. Chakraborty and S. Cant, Combustion and flame **137**, 129 (2004).

[44] N. Chakraborty, E. Hawkes, J. Chen, and R. Cant, Combustion and Flame **154**, 259 (2008).

[45] N. Chakraborty and M. Klein, Phys. Fluids **20**, 065102 (2008).

[46] N. Chakraborty and R. Cant, Physics of Fluids **17**, 105105 (2005).

[47] Y. Gao and N. Chakraborty, Numerical Heat Transfer, Part A: Applications **69**, 1201 (2016).

[48] Y. Gao, Y. Minamoto, M. Tanahashi, and N. Chakraborty, Combustion Science and Technology **188**, 1398 (2016).

[49] N. Chakraborty, H. Kolla, R. Sankaran, E. Hawkes, J. Chen, and N. Swaminathan, Proceedings of the Combustion Institute **34**, 1151 (2013).

[50] S. R. Muppala, N. K. Aluri, F. Dinkelacker, and A. Leipertz, Combustion and Flame **140**, 257 (2005).

[51] H. Kobayashi, T. Tamura, K. Maruta, T. Niioka, and F. A. Williams, in *Symposium (International) on Combustion* (Elsevier, 1996), vol. 26, pp. 389–396.

[52] C. Law and O. Kwon, International Journal of Hydrogen Energy **29**, 867 (2004).

[53] F. Dinkelacker, B. Manickam, and S. Muppala, Combustion and Flame **158**, 1742 (2011).

[54] T. Poinsot and S. Lele, NASA Comput. Phys. **101**, 104–129 (1992).

[55] A. Wray, Report No. MS 202 A-1 - NASA Ames Research Center (1990).

[56] T. Poinsot and D. Veynante, *Theoretical and numerical combustion* (RT Edwards, Inc., 2005).

[57] M. Boger, D. Veynante, H. Boughanem, and A. Trouvé, Proc. Combust. Inst. **27**, 917–925 (1998).

[58] N. Chakraborty and R. Cant, Combust. Flame **156**, 1427 (2009).